

Copyright

By

Andrew Peter Wang

2014

The Thesis Committee for Andrew Peter Wang  
Certifies that this is the approved version of the following thesis:

**Wireless Power Transmission and Communication System for Implantable  
Devices in Rodents**

**APPROVED BY**  
**SUPERVISING COMMITTEE**

**Supervisor:** \_\_\_\_\_

Jonathan W. Valvano

**Co-Supervisor:** \_\_\_\_\_

John A. Pearce

**Wireless Power Transmission and Communication System for Implantable  
Devices in Rodents**

**by**

**Andrew Peter Wang, B.S.E.E.**

**Thesis**

Presented to the Faculty of the Graduate School of

The University of Texas at Austin

in Partial Fulfillment

of the Requirements

for the Degree of

**Master of Science in Engineering**

**The University of Texas at Austin**

**December 2014**

## Acknowledgements

The pursuit of my electrical engineering degrees have been filled with many successes and failures, but most of all, a constant struggle to reach my goals. The journey to achieving ones goals has many different paths and can sometimes become unclear. I was told by Dr. Jonathan Valvano, after being given a list of things to do, to most importantly be happy. During one of my periods of struggle, these words stuck and I realized that being happy makes the journey to achieving my goals more clear and that a period of struggle can be enjoyed even though it is often perceived in a negative connotation. I would like to acknowledge all of the people who have helped me through my struggles because they often lead to successes in my life.

I would like to thank *Dr. Jonathan Valvano* for giving me the opportunity to work in his lab and for being such a supportive advisor. Dr. Valvano cares about the bigger picture for the wellbeing of his students and does not have an ego. I have had a more enjoyable time in school pursuing my degree than most graduate students because of his guidance, genuine care, and lively character.

I would like to thank *Dr. John Pearce* for giving me the opportunity to work in his lab and as his teaching assistant. Taking Dr. Pearce's biomedical instrumentation class was what made me decide that I wanted to pursue electrical engineering for my career. It is amazing how Dr. Pearce is knowledgeable in not only the ECE, but the ME and BME worlds. I can't count how many times I have said, "Well, Dr. Pearce was right" and when working on circuits. Like Dr. Valvano, Dr. Pearce also genuinely cares about the progress of his students. I also appreciate all the funny life stories he shares randomly during class or in his office.

I would like to thank *Kelvin Le* for being such an awesome research partner and friend. Kelvin is extremely skilled technically and I have gone to him many times for advice on designs. He also brings character into the research lab which creates a lively atmosphere.

I would like to thank *Lucas Holt* for making me more productive just by observing his efficiency in completing his work. Thank you for also bringing character into the research lab and for all the times we've sat and pondered solutions to problems. Your energy and enthusiasm motivates the people around you.

I would like to thank *Ben Bright* for helping me start this project and teaching me to pay attention to detail.

I would like to thank *Kaarthik Rajendran* for helping me with this project starting last summer and being a great research partner.

I would like to thank *Dr. Guru Khalsa* for helping me with the Helmholtz coil design and giving me advice on life.

Lastly, to my Dad *Peter Wang*, Mom *Shin-Fei Wang*, and my sister *Diana Wang* I truly appreciate their guidance, love, and support. My dad never stops guiding me in the right direction and believing in me. He always taught me to aim for the stars, be a good human being, and seek the truth. My mom has always cared for me and is a very happy and bubbly person who always puts me in a good mood. My sister is someone who I can talk to about anything and I respect her for all her achievements. I am competitive with her but in the end we are on the same side.

## **Abstract**

# **Wireless Power Transmission and Communication System for Implantable Devices in Rodents**

Andrew Peter Wang, M.S.E.

The University of Texas at Austin, 2014

Supervisor: Jonathan W. Valvano

Co-Supervisor: John A. Pearce

Measuring physiological changes in rodents helps determine drug safety and efficacy in the pharmaceutical industry. This has led to the miniaturization of implantable devices for rodents to reduce the physical stress on the animals. The most common power source for implantable devices are batteries, which are heavy, take up space, and need to be replaced. In this thesis, an inductive power and communication link system has been designed to eliminate the need of a battery and reduce the size of the implantable device for rodents. Power is transmitted by inductive coupling from a Helmholtz primary coil, which is wrapped vertically along the rodent's cage, to the implant secondary coil. Communication from the implant to the base station is achieved by impedance modulation of the implant transmitter coil back to the base station primary coil. This method of communication eliminates the need for a bulky antenna and reduces power consumption. The proposed design can successfully power the implant in a 5350cc cage while it sends temperature data to the base station at 10Hz. The implant is 1.32cc in size and consumes 10.25mW of power while taking and transmitting temperature data.

## Table of Contents

Table of Contents .....	vii
List of Figures .....	ix
List of Tables .....	xi
Chapter 1: Introduction .....	1
1.1 Motivation.....	1
1.2 Design Objectives .....	2
1.3 Theory of the Inductive Power Link.....	5
1.4 Theory of Impedance Modulation .....	7
Chapter 2: Implementation .....	9
2.1 System.....	9
2.2 System Power.....	10
2.2.1 Power Circuit: Primary .....	10
2.2.1.1 Oscillator Circuit.....	11
2.2.1.2 Class E Power Amplifier .....	14
2.2.2 Power Circuit: Secondary .....	18
2.2.2.1 Cockroft-Walton Voltage Multiplier .....	19
2.3 System Communication .....	21
2.3.1 Communication Circuit: Transmitter.....	22
2.3.2 Communication Circuit: Receiver .....	24
2.4 Physical Design.....	26
2.4.1 Base Station Design .....	26
2.4.2 Implant Design.....	32

2.5 Temperature Data.....	34
Chapter 3: Verification and Results .....	35
3.1 Measurement Analysis.....	35
3.2 Range and Power Consumption.....	40
3.3 Noise Analysis .....	41
Chapter 4: Conclusion.....	43
4.1 System Performance .....	43
4.2 Future Directions .....	44
4.2.1 Data Frequency .....	44
4.2.2 Communication Protocol .....	44
4.2.3 Half-Duplex Communication.....	45
4.2.4 Automatic Gain Control.....	45
4.2.5 Alternative Coil and Cage Structure .....	46
References .....	47



## List of Figures

Figure 1: Current Consumption during Different Modes of Operation .....	3
Figure 2: Circuit Model for Inductive Coupling [4] .....	6
Figure 3: Block Diagram of Inductive Coupling Circuit Model [4] .....	6
Figure 4: System Block Diagram.....	9
Figure 5: Primary Power Circuit Block Diagram .....	10
Figure 6: Oscillator Block Diagram [5] .....	12
Figure 7: Crystal Oscillator Circuit Model .....	12
Figure 8: Edge Triggered D-FlipFlop .....	13
Figure 9: Class E Power Amplifier Circuit Model .....	15
Figure 10: Class E Power Amplifier ON State .....	16
Figure 11: Class E Power Amplifier OFF State.....	17
Figure 12: Class E Power Amplifier Current and Voltage Plots [7].....	18
Figure 13: Secondary Power Circuit Block Diagram .....	18
Figure 14: Half-Stage of Voltage Multiplier .....	19
Figure 15: Full Stage of Voltage Multiplier .....	20
Figure 16: Cochroft-Walton Voltage Multiplier.....	21
Figure 17: System Communication Block Diagram .....	22
Figure 18: Transmitter Circuit Model.....	23
Figure 19: Amplitude Modulated Power Signal .....	23
Figure 20: Receiver Block Diagram .....	24
Figure 21: Demodulation Diagram .....	25
Figure 22: Signal Conditioning Block Diagram .....	25
Figure 23: Copper Clad Prototyping .....	27
Figure 24: Magnetic Field of Single Loop and Helmholtz Coil [9][10].....	28
Figure 25: Cage Structure .....	29
Figure 26: Helmholtz Coil Diameter .....	30
Figure 27: Helmholtz Coil Separation Distance .....	31
Figure 28: Copper Shielded Enclosure .....	31
Figure 29: Implant Dimensions .....	33
Figure 30: Implant Coil Structure .....	33
Figure 31: Overall Coil Efficiency with respect to Coil Distance .....	34
Figure 32: Crystal Oscillator and D-FlipFlop Output.....	35
Figure 33: Gate Driver and Drain Signal Output.....	36
Figure 34: 6.78MHz Amplitude Modulated Power Signal .....	36
Figure 35: Reduced 6.78MHz Power Signal and Half-Wave Rectified Output .....	37
Figure 36: Demodulated Data Signal.....	38
Figure 37: Data Signal .....	38

Figure 38: FFT of Data Signal with 60Hz, 120Hz, and 6.78MHz Noise .....	39
Figure 39: Implant Coil Magnitude and Phase Plot.....	40
Figure 40: Communication Protocol.....	45

## List of Tables

Table 1: Market Analysis of Competitive Devices .....	3
Table 2: Design Objectives .....	4
Table 3: Achieved Design Objectives.....	43

# Chapter 1: Introduction

## 1.1 Motivation

Interest in implantable devices has been rapidly increasing in recent years. In the medical field, there are pacemakers for cardiac arrhythmia, spinal stimulators, retinal implants, cochlear implants, and other devices that can monitor physiological signals and stimulate tissue.

Implantable devices are also seen in the pharmaceutical industry, where new drugs are tested on rodents, such as mice and rats, and their physiological signals are monitored in order to observe the effects of the new drugs. One example requiring the need for monitoring is the testing of new cardiac drugs. Heart disease is the leading cause of death in the United States [1]. The ability to observe the changes in cardiac function of the rodents is a key factor in the development of these new drugs and has resulted in the creation of implantable devices that can wirelessly transmit cardiac data such as left ventricular stroke volume and pressure to a base station [2].

Furthermore, even noncardiac drugs must be tested for possible effects on cardiac function.

Typically, these drugs are tested in rodents.

The typical implant used for rodent measurements consists of circuitry required to monitor physiological signals, power the implant, and wirelessly communicate. The most common power source for an implantable device is a battery. Batteries have limited lifetimes, require recharging, and will eventually need to be replaced. Also, the space the battery takes up makes it difficult to reduce the implant to a size that is suitable for rodents. Tradeoffs are encountered among the size, power, and communication circuitry of the implant that eventually leads to the need for a

low power design. For example, equation 1.1 shows that  $E$  is the battery storage specification in amp-hours and  $t_{life}$  is length of time the implant can operate [2].

$$Average\ Current \leq \frac{E}{t_{life}} \quad (1.1)$$

Reducing the required average current needed to operate the implant, which the communication circuitry largely consumes, will reduce the battery storage specification and battery size in order to operate the implant for the desired  $\tau_{life}$ . The goal of this work is to miniaturize implantable devices to reduce the physical strain on rodents by eliminating the battery as a power source and alternatively power the implant via inductive coupling between two coils. Also, a more power-efficient design will be implemented for wireless communication via impedance modulation by tuning and detuning a coil to create a form of amplitude modulation. This proposed solution will not only allow for a lighter and smaller sized implant, but also a lower power design.

## 1.2 Design Objectives

Table 1 is a list of the specifications of implantable devices currently on the market that measure biological signals in animals [3]. Notice that only the UT Austin implant can take cardiac volume measurements. Figure 1 shows the instantaneous current consumption during operation of the UT Austin implant.

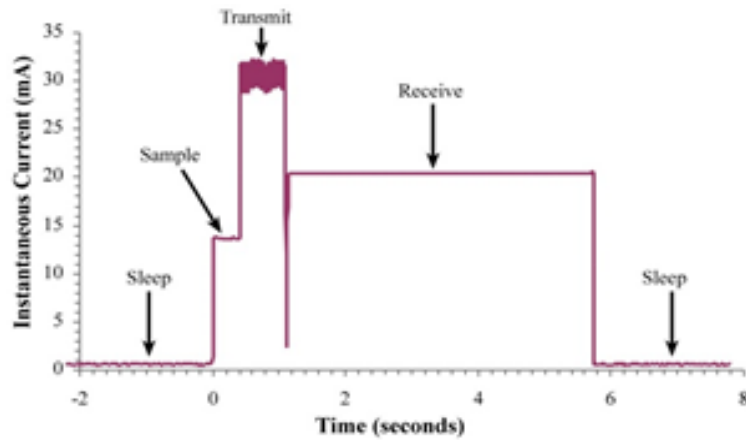






Figure 1: Current Consumption during Different Modes of Operation

Table 1: Market Analysis of Competitive Devices

Parameter	Millar	Transonic	Data Sciences	UT Austin
				
Size	5-6 cc est.	25 cc	1.4 cc	5 cc
Battery Life	Inductive Power	2-6 weeks continuous, 6mo. Low pwr.	1 month	2 month at 43 collections/day
Measurements Available	Pressure, SNA, ECG, EMG, EEG, temperature	Flow, blood pressure, ECG, temperature	Pressure, ECG, EEG, EOG, EMG, temperature, "activity"	Pressure, Volume, Cardiac Output
Pressure Range	-20 to 300 mmHg	-50 to 300 mmHg	-20 to 300 mmHg	-40 to 400 mmHg
Pressure Resolution				0.4 mmHg
Pressure Accuracy			+/- 3 mmHg	
Pressure Drift			<2 mmHg/mo.	± 3 mmHg
Sampling Frequency	2 kHz, or 8kHz	120 Hz, or 60 Hz	Biopotential bandwidth: 200 Hz	1 kHz
Communication Protocol	Inductive	RF	RF	RF

The goal of this wireless power transmission and communication system is to transmit temperature data from an implant to a base station with design objectives specified in Table 2. The implant was sized to be smaller than the Data Sciences implant that is currently the smallest on the market at 1.4cc. The operational frequency was chosen to be 6.78MHz, which is the lowest band in the industrial, scientific, and medical allocated radio bands. Parasitic effects become more prevalent at higher frequencies of operation, which led to the choice of the lower frequency option. The data transmission rate was chosen to be 10Hz, for ease of design in the receiver portion of the circuit, and is sufficient for temperature measurements. The current consumption must be reduced below 20mA, which is the minimum current consumption that the UT Austin implant consumes while transmitting and receiving data. The operational volume is specified to be 5350cc, which is similar in size to a small mouse cage. Simplex communication from the implant to the base station is pursued in this prototype and half-duplex can be implemented in the future.

Table 2: Design Objectives

Size	<1.4cc
Operational Frequency	6.78MHz
Data Frequency	10Hz
Power Consumption (while transmitting)	<20mA
Cage Volume	5350cc
Communication Channel	Simplex

### 1.3 Theory of the Inductive Power Link

When a constant magnetic field is produced by a coil there is no voltage induced on the coil assuming no resistive losses. However, if the magnetic field on the coil is time-varying, a voltage will be created in order to counter the change of the magnetic field on the coil causing current to flow. The voltage or electromotive force (emf)  $V$  induced on the coil due to a time-varying magnetic field is shown in Faraday's Law in equation 1.2.  $B$  is the magnetic field,  $A$  is the surface area of the coil,  $N$  is the number of turns of the coil, and  $t$  is time. Notice that the polarity of the emf is negative because the coil wants to maintain a constant magnetic flux ( $BA$ ) and create an induced magnetic field to counter the change in the magnetic field according to Lenz's Law.

$$V = -N \frac{\Delta(BA)}{\Delta t} \quad (1.2)$$

In the system, two coils will be used, where the primary coil creates the changing magnetic field inducing a voltage on the secondary coil, which in turn powers the implant. Shown in equation 1.3, the mutual inductance  $M$  relates the change in current  $I_{prim}$  from the primary coil needed to create the magnetic field to the voltage  $V_{sec}$  produced on the secondary coil.  $M$  can be calculated in equation 1.4, where  $L_1$  and  $L_2$  are the self-inductances of the primary and secondary coils, respectively, and  $k$  is the coupling coefficient described in more detail below.

$$V_{sec} = -M \frac{\Delta I_{prim}}{\Delta t} \quad (1.3) \quad M = k\sqrt{L_1 L_2} \quad (1.4)$$



Shown below in Figure 2 and 3, is the circuit model and block diagram of the inductive power link taken from reference [4]. The changing magnetic field is produced on the primary coil self-inductance  $L_1$  using a series LC tank circuit causing the L impedance and C impedance to cancel out at the resonant frequency leaving only the coil resistance  $R_1$  shown in equation 1.5. The low impedance at the resonant frequency  $\omega_{res}$ , shown in equation 1.6, allows ac current to flow through the primary coil creating a changing magnetic field at the resonant frequency.

$$j\omega_{res}L + \frac{1}{j\omega_{res}C} = 0 \quad (1.5)$$

$$\omega_{res} = \frac{1}{\sqrt{LC}} \quad (1.6)$$

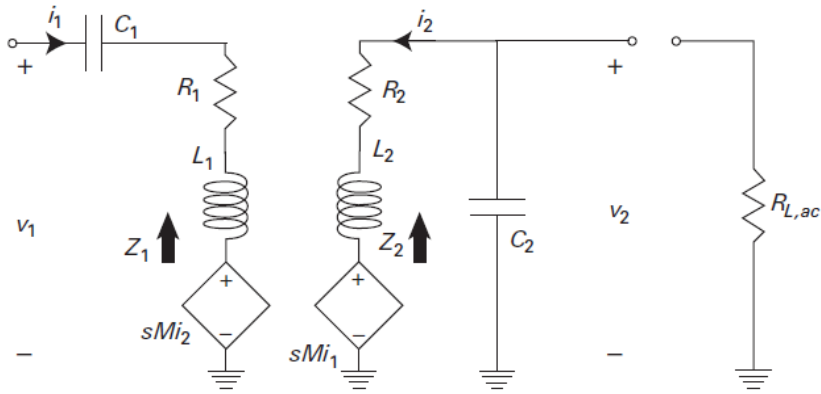


Figure 2: Circuit Model for Inductive Coupling [4]

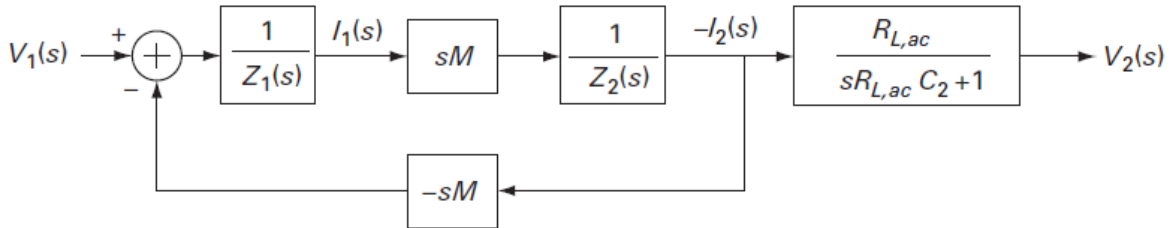


Figure 3: Block Diagram of Inductive Coupling Circuit Model [4]

On the implant side, a parallel LC tank circuit is tuned to the same resonant frequency as the primary coil where the secondary coil is represented by  $L_2$  and resonates with  $C_2$ . The parallel LC tank amplifies the induced voltage on the coil because at the resonant frequency the impedance theoretically goes to infinite, but is finite due to coil losses.  $R_2$  represents the coil resistance and  $R_L$  represents the resistance of the other implant circuitry (i.e. the load). The mutual inductance effects are modeled with the controlled source  $sMi_1$ , which is the voltage induced on the secondary coil due to the current in the primary coil, and controlled source  $sMi_2$ , which is the voltage induced on the primary coil due to the current in the secondary coil. The coupling coefficient  $k$  shows that the distance between the coils and the structure of the coils largely determines the efficiency of power transfer, where  $a$  is the coil radius,  $d$  is the coil wire diameter, and  $r$  is the distance between the two coils [4].

$$k = \frac{M}{\sqrt{L_1 L_2}} = \frac{\pi}{2 \sqrt{\ln\left(\frac{a_1}{d_1}\right) \ln\left(\frac{a_2}{d_2}\right)}} \left( \frac{a_1 a_2}{r^2 + a_1^2} \right)^{\frac{3}{2}} \quad (1.7)$$

#### 1.4 Theory of Impedance Modulation

The method of impedance modulation communication goes back to the circuit model and block diagram in Figures 2 and 3 [4]. Notice that a voltage is not only induced on the secondary coil, but also induced back to the primary coil in a feedback loop represented by the controlled source  $sMi_2$ . The effective impedance  $Z_{in}$  of the primary circuit can be modeled with equation 1.8 with loop transfer function  $H(s)$ .

$$Z_{in}(s) = Z_1(s)(1 - H(s)) \quad (1.8) \quad H(s) = \frac{M^2 s^2}{Z_1(s)Z_2(s)} \quad (1.9)$$

The primary circuit impedance change due to the feedback loop caused by the induced voltage from the secondary coil is called the reflected impedance  $Z_{ref}$ .

$$Z_{in}(s) = Z_1(s) + Z_{ref}(s) \quad (1.10) \quad Z_{ref}(s) = -\frac{M^2 s^2}{Z_2(s)} \quad (1.11)$$

Communication between the secondary coil and the primary coil is now possible if the reflected impedance  $Z_{ref}$  can be toggled corresponding to the data signal. This can be done by tuning and detuning the parallel LC tank circuit from the resonant frequency causing the reflected impedance to change and therefore altering the effective impedance of the primary circuit. This impedance change will modulate the voltage signal on the primary coil, which can then be demodulated and conditioned to obtain the data signal described in detail later.

## Chapter 2: Implementation

### 2.1 System

Figure 4 is a block diagram of the system that includes the implant and the base station. In both the implant and the base station, power and communication are the two major functional blocks required for proper operation. On the implant side, there is a coil that powers the microcontroller and takes readings from an internal temperature sensor. A separate coil in the implant is used to transmit the temperature data to the base station. The base station only has one coil, which is responsible for providing power for the implant, but also acts as the receiver for the data signal sent from the implant. Each functional block will be described in more detail.

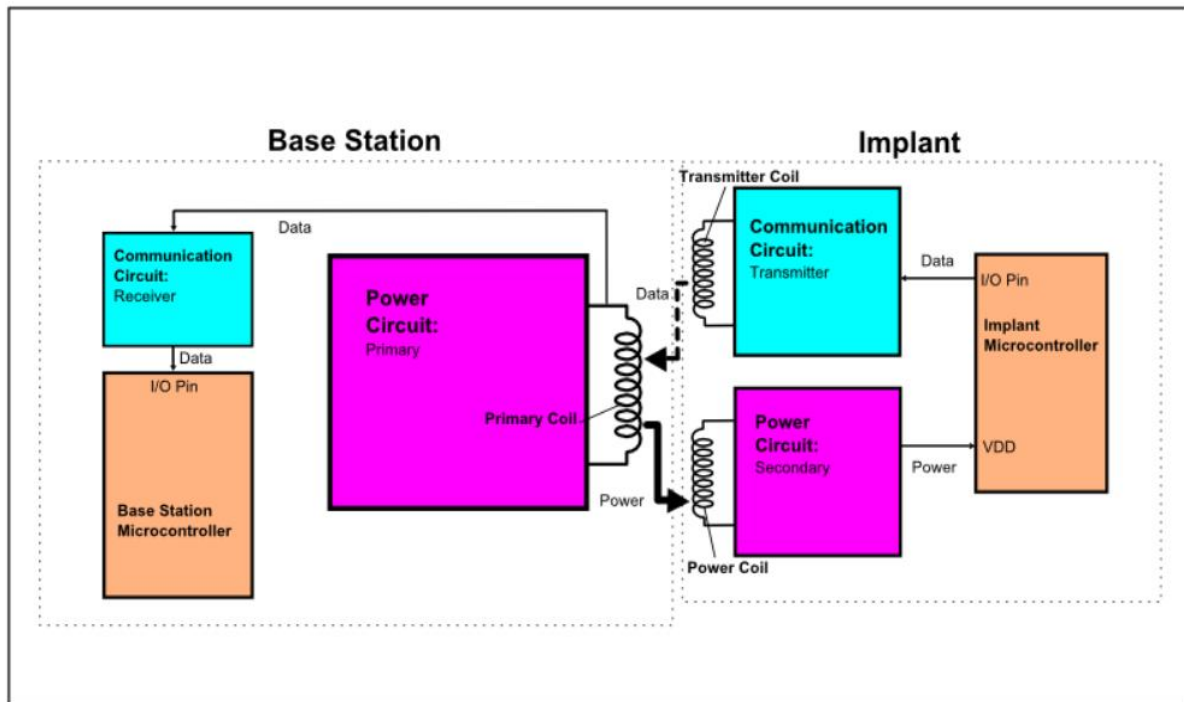


Figure 4: System Block Diagram

## 2.2 System Power

The system power is grouped into the “Power Circuit: Primary” on the base station and “Power Circuit: Secondary” on the implant, as shown above in Figure 4. The base station circuitry is powered by either a 12V battery or regulated wall power supply. The primary power circuit on the base station sends current to the primary coil, which transfers power from the primary coil to the secondary coil via inductive coupling. The induced current on the secondary coil is then regulated by the secondary power circuit, which then provides power for the microcontroller.

### 2.2.1 Power Circuit: Primary

The primary power circuit is composed of an oscillator circuit, which generates a 6.78MHz square wave signal to drive the MOSFET of a class E power amplifier, as shown in Figure 5. The class E power amplifier is a non-linear, switching mode amplifier with a theoretical power efficiency of 100%. The class E power amplifier sends AC current at the frequency of operation into the primary coil in order to generate a magnetic field for inductive coupling to the implant secondary coil.

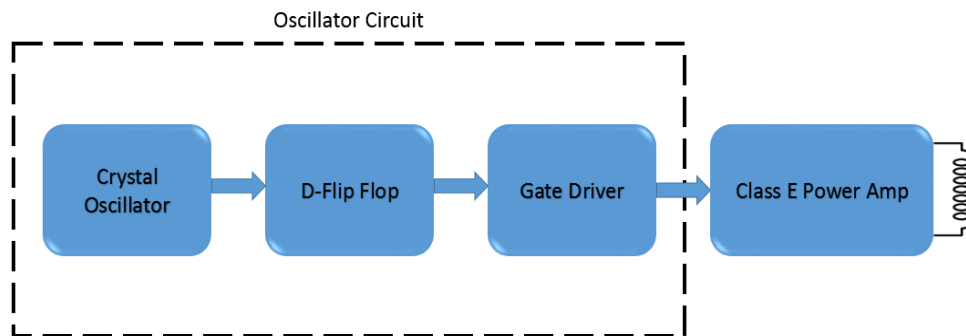


Figure 5: Primary Power Circuit Block Diagram

### 2.2.1.1 Oscillator Circuit

The oscillator circuit is composed of three major components: a crystal oscillator, a D-flip flop, and gate driver (Figure 5). The crystal oscillator is used to generate a 13.56MHz square wave, which is fed into the D-flip flop for frequency division creating the 6.78MHz frequency of operation. The gate driver is needed to provide a high drive current for the transistor of the power amplifier due to the fast switching time required for 6.78MHz operation and to reduce power loss in the transistor.

The basic operation of an oscillator can be modeled as an amplifier and filter in a positive feedback loop, as shown in Figure 6. The filter block, in this case, is the crystal with a resonant frequency of 13.56MHz. In order for the circuit to begin oscillation, it must satisfy the Barkhausen Criteria [5]:

1. Loop gain is equal to unity at the resonant frequency
2. Phase shift around the loop is  $n2\pi$  radians where  $n$  is an integer

The filter block contributes a 180 degree phase shift, which requires the amplifier block to be an inverting amplifier in order to achieve a 360 degree phase shift to satisfy criteria (2). If criterion (1) is satisfied, then a positive feedback loop will be created. When power is applied to the circuit, the voltage change excites the resonant frequency of the filter block and the signal is multiplied by the amplifier block until the nonlinearities of the amplifier cause the signal to reach steady state. If the loop gain is greater than unity, then growth of the signal to steady state operation is faster.

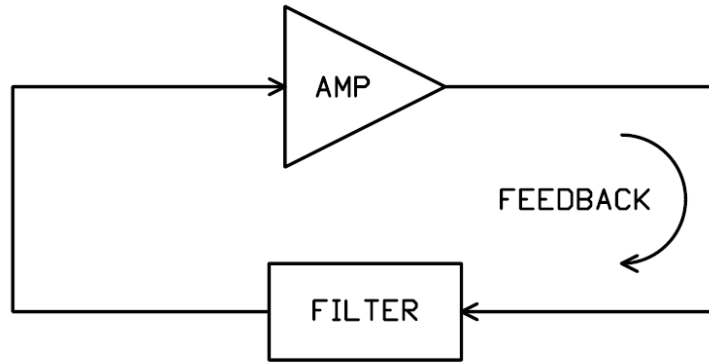


Figure 6: Oscillator Block Diagram [5]

The stable frequency requirement of exactly 6.78MHz leads to the choice of a crystal for the filter block instead of an LC network. An LC network resonant frequency tends to be more sensitive to power supply voltage, temperature, and mechanical vibrations. This requires tuning of the LC network; whereas, the crystal natural resonant frequency is very stable. A crystal can be modeled as an RLC circuit, as shown in Figure 7.

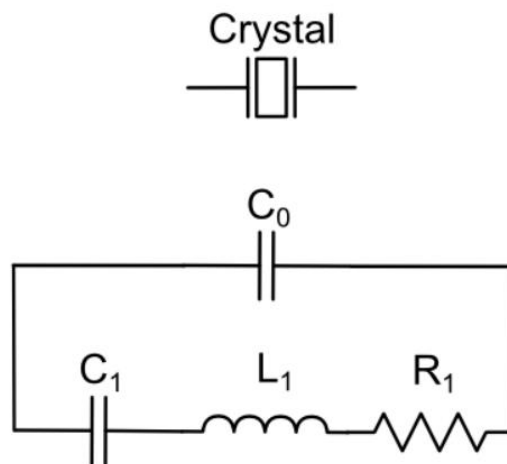


Figure 7: Crystal Oscillator Circuit Model

- $C_0$  = Sum of capacitance due to the electrodes on the crystal plate plus stray capacitances due to the crystal holder and enclosure.
- $C_1$  = Motional arm capacitance. Elasticity, shape, and area of the crystal.
- $L_1$  = Motional arm inductance. Vibrating mechanical mass of the crystal.
- $R_1$  = Resistive losses in the crystal.

Due to product availability, a 13.56MHz crystal is chosen and therefore requires a frequency divider in order to obtain the 6.78MHz operating frequency. This can be done by using a single edge triggered D-flip flop. Shown in Figure 8, the D port is captured during a specific edge of the input clock cycle and in turn makes the Q port the same value. The Q value will stay the same until the next specific edge on the clock triggers a change. In order to perform frequency division, the D port is connected to the inverse of Q port. The Q port can only change to the value of the D port when there is another edge on the clock signal (output of crystal oscillator in this case). The D port will always change to the inverse of the Q port during an edge trigger which creates a square wave output at the Q port that is half the frequency of the output signal of the crystal oscillator.

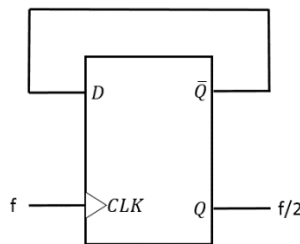


Figure 8: Edge Triggered D-FlipFlop



Now that the 6.78MHz square wave signal has been obtained, the amount of current that is output to the power amplifier stage needs to be increased with the gate driver block. The class E power amplifier that is used in this device requires a power MOSFET to be switched on and off at the frequency of operation. The gate of the transistor forms a capacitor that needs to be charged and discharged each time the transistor switches on and off. In order to switch at a frequency of 6.78MHz, sufficient current must be sent into the gate to achieve a proper switching frequency in the transistor. If insufficient current is sent into the gate, the switching speed will be too slow (due to gate capacitance) and the transistor will have power loss due to simultaneous voltage and current on the transistor [6].

#### **2.2.1.2 Class E Power Amplifier**

The class E power amplifier is a non-linear, switching mode amplifier chosen due to its theoretical power efficiency of 100%. The difference between linear and switching mode amplifiers is that the linear amplifier output power is dependent on the input amplitude whereas a switching mode amplifier's output power is a function of the switching activity of the input. The conduction angle is defined in equation 2.1, where  $\alpha_1$  is the period of time when the switch is closed and conducting current in the positive direction and  $\alpha_2$  is an arbitrarily chosen duration when the switch is open and the current is drops.

$$\varphi = \alpha_1 + \alpha_2 \quad (2.1)$$

The general circuit model of a class E power amplifier consists of a common source amplifier with an inductor choke and an LC series tank matching network as shown in Figure 9.

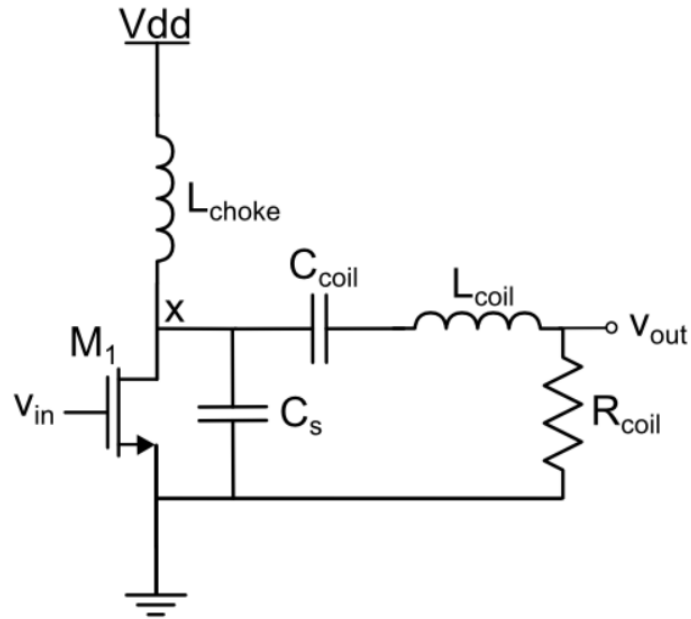


Figure 9: Class E Power Amplifier Circuit Model

- $M_1$  = Power MOSFET
- $L_{\text{coil}}$  = Primary coil
- $R_{\text{coil}}$  = Resistance of primary coil
- $C_{\text{coil}}$  = Capacitor for tuning series resonant LC tank
- $L_{\text{choke}}$  = RF choke inductor
- $C_s$  = junction capacitance of  $M_1$  and parasitic capacitance of  $L_{\text{choke}}$

As the name implies, the transistor  $M_1$  acts as a switch rather than a voltage-dependent current source (i.e. between the triode and cut off and not in the saturation region). In order to achieve high efficiency, (1)  $M_1$  must sustain a small drain to source voltage  $v_{ds}$  when it carries current, (2)  $M_1$  carries a small current when a finite voltage is sustained, and (3) there is minimal

transition time between the on and off states of  $M_1$  [7]. Criterion (3) explains why a square wave input signal with minimal transition time was generated, versus a sinusoidal input signal. The gate driver from the previous stage also helps optimize criterion (3) because it compensates for the input gate-capacitance transition delay. Analysis of the “on” and “off” states of the amplifier, shown in Figures 10 and 11, makes the optimization of criteria (1) and (2) more clear.

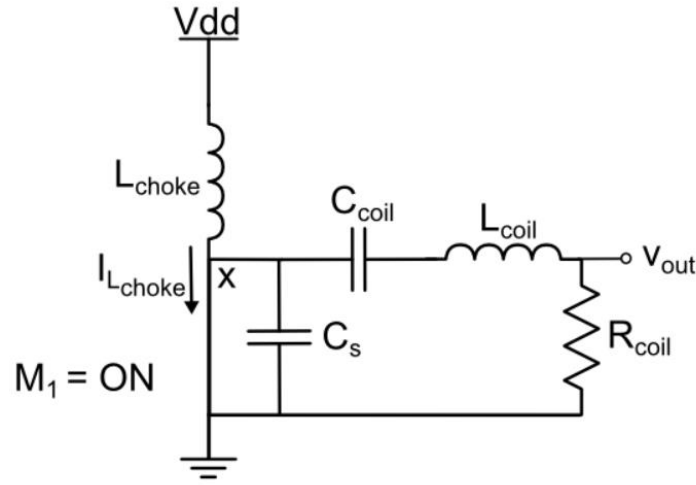


Figure 10: Class E Power Amplifier ON State

When  $M_1$  is on, the transistor is a low-resistance channel and the voltage at node X is pulled near ground causing a large voltage drop across  $L_{choke}$  and creating the current  $I_{Lchoke}$  in equation 2.2.

$$I_{Lchoke} = \frac{1}{L_{choke}} \int (Vdd - X) dt \approx \frac{Vdd - X}{L_{choke}} t \quad (2.2)$$

When  $M_1$  is off, the transistor acts as an open circuits (the MOSFET is cut off) which allows  $I_{Lchoke}$  to charge up  $C_s$  and then the voltage at node X will rise. The rising voltage at node X will excite the series resonant LC tank circuit causing an AC current at the frequency of operation to

flow in the primary coil. This AC current also brings the voltage at node X back to ground before the transistor is switched on again.

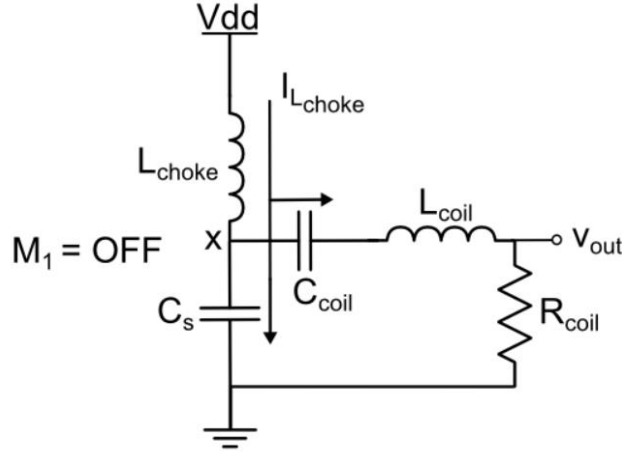


Figure 11: Class E Power Amplifier OFF State

Figure 12, taken from [7], summarizes the operation of the class E amplifier where  $I_{LD} = I_{Lchoke}$ . During the first half-cycle, where the input signal is high, the transistor turns on and  $L_{choke}$  is charged. This satisfies criterion (1) because the voltage at node x is pulled to ground while there is current flowing in the transistor. During the next half-cycle, when the input signal is low, the transistor turns off causing the voltage at node X to rise and eventually drop due to the resonant circuit. This satisfies criterion (2) because there is no current flowing through the transistor during the “off” stage, while there is now a finite voltage at node X. Notice that  $C_s$  allows node X to be held at ground for a very short time while it is being charged, allowing the transistor to fully turn “off” before node X rises. Further, node X and  $I_{Lchoke}$  are zero before the transistor

turns “on” again. The series resonant LC tank acts as a filter at the operating frequency that creates a clean sinusoidal waveform at the output.

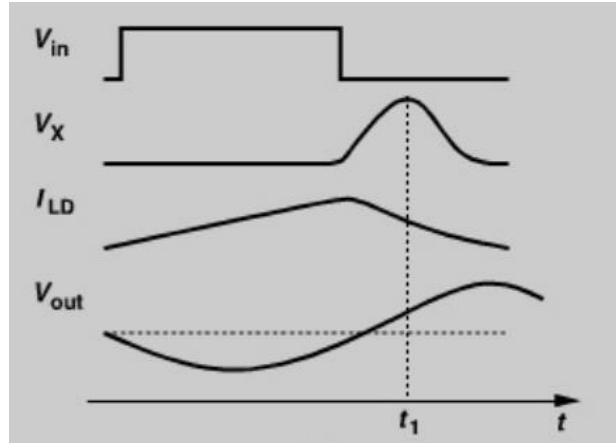


Figure 12: Class E Power Amplifier Current and Voltage Plots [7]

### 2.2.2 Power Circuit: Secondary

After the magnetic field is generated from the primary coil in the power amplifier, an inductive power link, described in chapter 1, is created with the secondary power circuit on the implant as shown in Figure 4. The secondary power circuit consists of a parallel LC tank circuit, Cockroft-Walton voltage multiplier, and a regulator shown in Figure 13.

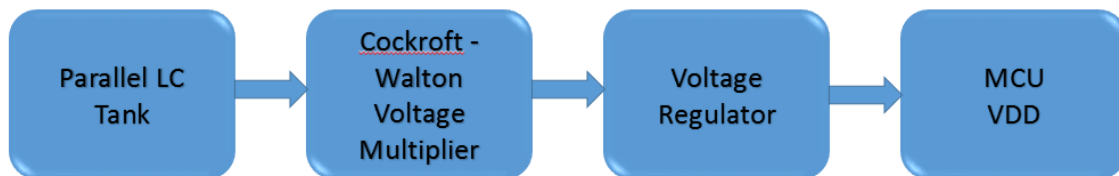


Figure 13: Secondary Power Circuit Block Diagram

As described in Chapter 1, the parallel LC tank has a high impedance at its resonant frequency. Therefore, the voltage created across the parallel LC tank will be at its highest when the frequency of the magnetic field and the resonant frequency of the parallel LC tank are the same. Due to the distance and angle of orientation of the secondary coil with respect to the primary coil, the voltage seen across the parallel LC tank may be small, depending on the amount of current induced in the secondary coil. The problem can be solved by using a Cockcroft-Walton voltage multiplier, which is also an AC-DC converter, before going into the regulator that provides the DC voltage needed to power the MCU.

### 2.2.2.1 Cockcroft-Walton Voltage Multiplier

The Cockcroft-Walton voltage multiplier not only multiplies the voltage seen across the parallel LC tank, but also converts the AC voltage signal to a DC voltage in the range of the voltage regulator. In the figures below,  $v(t)$  represents the AC voltage across the parallel LC tank circuit and diode voltage drops are ignored.

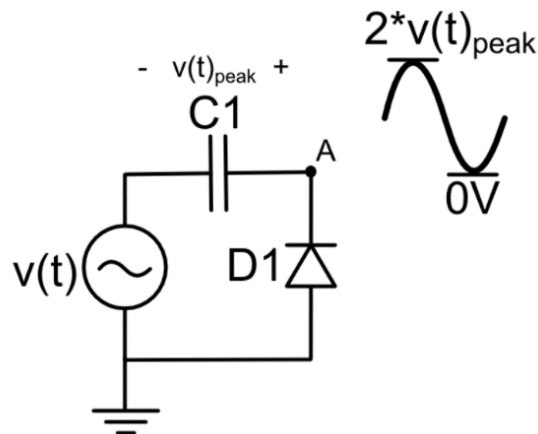


Figure 14: Half-Stage of Voltage Multiplier

During the negative half-cycle of  $v(t)$ , D1 is forward-biased and charges C1 to  $v(t)_{\text{peak}}$ . When  $v(t)$  reaches the positive half-cycle, D1 is “off” in the reverse-biased mode causing the voltage on node A to be  $v(t)_{\text{peak}}$  from the input added to the charge stored on C1 which equals  $2*v(t)_{\text{peak}}$ . When the negative half-cycle of  $v(t)$  occurs again, D1 is conducting, causing node A to be driven to ground which gives us the sinusoidal waveform shown in Figure 14. If a rectifier composed of just a diode and capacitor is added to the circuit, diode D2 will conduct when node A reaches the positive half-cycle charging C2 to  $2*v(t)_{\text{peak}}$ . When node A is in the negative half-cycle, D2 is off causing the AC signal from node A to be rectified into a DC voltage that is twice  $v(t)_{\text{peak}}$  referred to as  $2*V_{\text{peak}}$ .

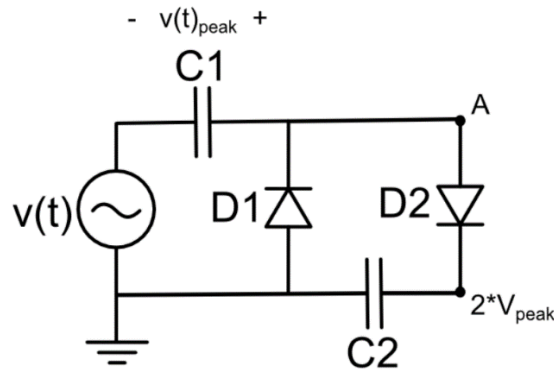


Figure 15: Full Stage of Voltage Multiplier

In order to multiply the voltage even further, a second replica of the circuit above can be connected in order to create  $4*V_{\text{peak}}$  as shown in Figure 16. The only difference in the second replica of the circuit is that the reference for the new circuit is now  $2*V_{\text{peak}}$ , which shifts up the AC signal from node A creating a  $4*v(t)_{\text{peak}}$  on node B. After the rectification, the output is now a DC voltage of  $4*V_{\text{peak}}$  sent to the voltage regulator [8].

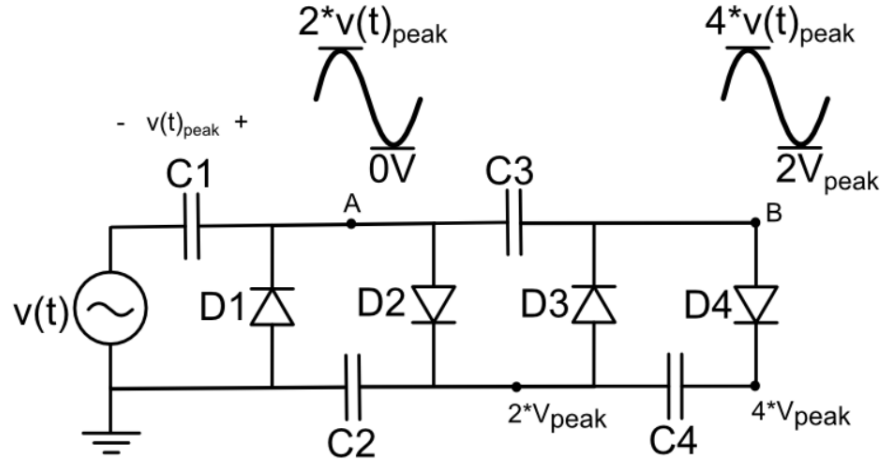


Figure 16: Cockcroft-Walton Voltage Multiplier

### 2.3 System Communication

In order for the implant to send data to the base station, the method of impedance modulation between the transmitter and primary coil is used. The transmitter coil is a separate coil from the power coil formed on the implant as shown in Figure 4. Having two coils decouples the communication and power portion of the implant circuitry, which allows the implant to be powered without interference from the transmitter coil while it is transmitting data. Note that the primary coil on the base station acts as both the receiver coil and the power coil. As shown in Figure 17, the implant transmitter amplitude modulates the data signal onto the primary coil on the base station via impedance reflection described in Chapter 1. The receiver circuit on the base station demodulates the data signal with analog signal conditioning before being sent to the base station MCU for further digital signal processing.



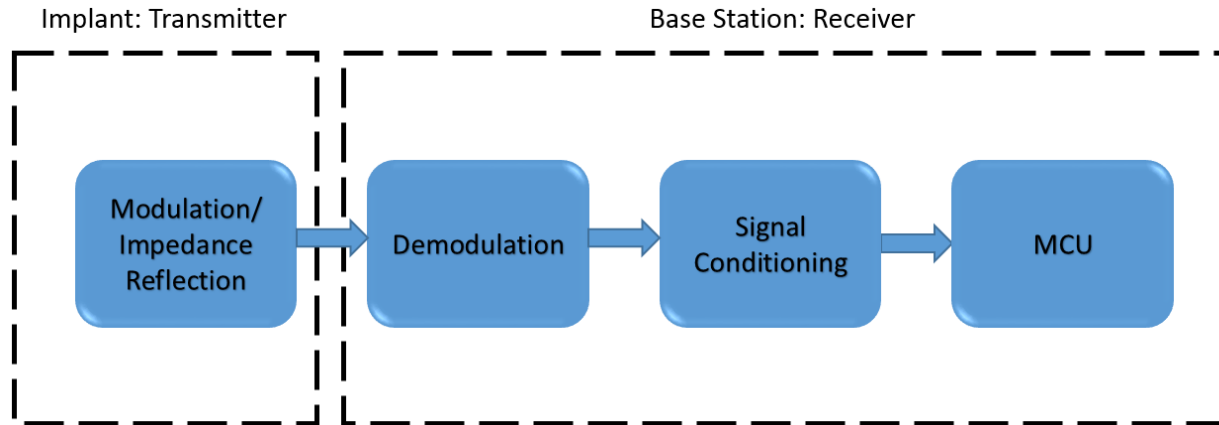


Figure 17: System Communication Block Diagram

### 2.3.1 Communication Circuit: Transmitter

The modulation of the data signal is implemented by using a switch to tune and detune the parallel LC tank circuit composed of the transmitter coil and a tuning capacitor, as shown in Figure 18. The switch is connected to the I/O port on the MCU, that contains the data signal. When the data signal is high, the switch will close causing the parallel resonant circuit to be tuned to the operating frequency of 6.78MHz causing the primary coil on the base station to see a reflected impedance. When the data signal is low, the switch is open and the transmitter coil is detuned from the operating frequency, which causes less of the impedance reflection mentioned in Chapter 1.

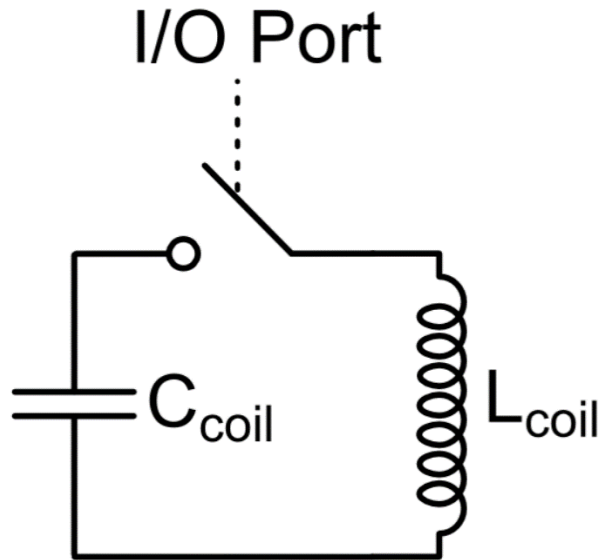


Figure 18: Transmitter Circuit Model

On the base station, the primary coil has a large voltage drop across it due to the large amount of AC current being sent into the coil for power. When the transmitter resonant circuit is in the tuned state, the voltage across the primary coil will drop due to the impedance reflection as shown below in Figure 19. This causes a modulated signal on the primary coil that corresponds to the data signal coming from the MCU port.

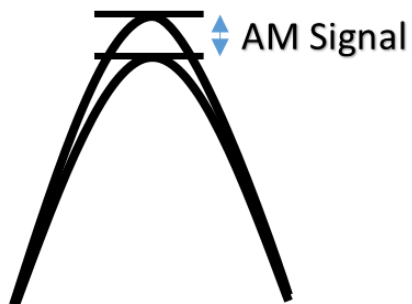


Figure 19: Amplitude Modulated Power Signal

### 2.3.2 Communication Circuit: Receiver

After the data signal is modulated onto the voltage on the primary coil, the receiver circuitry on the base station retrieves the data signal and sends it into the MCU. The first step in retrieving the data signal is to demodulate it. The voltage on the primary coil must first be reduced by a voltage divider to satisfy the input voltage range of the amplifiers to follow. The modulated voltage signal is now fed into a half-wave rectifier where the AC signal is converted to a DC signal. A half-wave rectifier was chosen instead of a full-wave rectifier because of the simplicity and ease of tuning in order to get the right waveform shape. The signal is then band-pass filtered in order to demodulate the data signal, as shown in Figure 20. The high pass filter will compensate for DC offsets in the circuitry and also low frequency movement from the rodent. The low pass filter will remove the 6.78MHz waveform and the square wave data signal will remain on the output of this stage shown in red in Figure 21.



Figure 20: Receiver Block Diagram

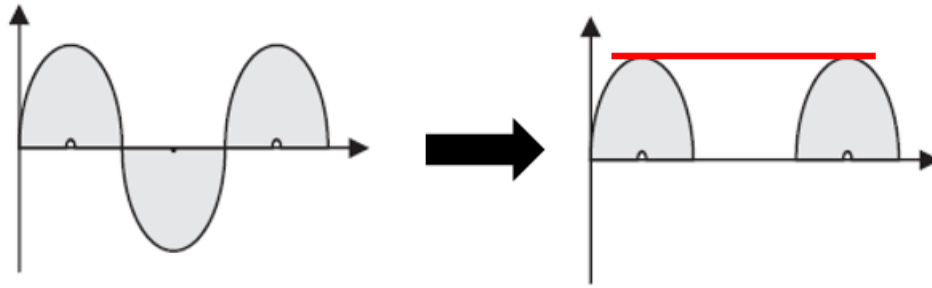


Figure 21: Demodulation Diagram

After the data signal is demodulated, its signal strength is low because of noise from external sources, such as the power line, ground plane noise, and the magnetic field from the power circuitry. In order to solve this problem, a gain stage is added to amplify the total signal that includes the noise and the data signal. After this is done, the noise is filtered out by a band-pass filter that outputs a larger amplitude data signal and increases signal strength into the MCU for further digital signal processing as shown in Figure 22. In summary, this stage amplifies the data signal while filtering out the noise.

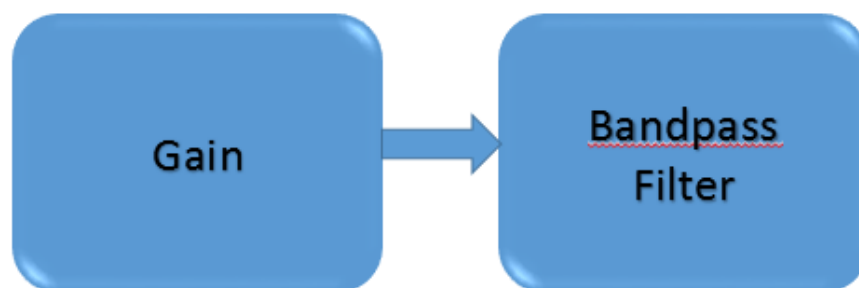


Figure 22: Signal Conditioning Block Diagram

## **2.4 Physical Design**

The physical design of this system must be adjusted to accommodate the living environment and size of the rodents. The base station must be designed in order to fit around the cage where the freely moving rodents live, and the implant must be small and light enough so that it does not physically constrain the rodent.

### **2.4.1 Base Station Design**

The base station circuitry was prototyped on copper cladding, shown in Figure 23, because the parasitic capacitance from breadboards have a strong effect at the 6.78MHz frequency of operation, and the copper cladding allows for an effective ground plane. The effective ground plane is needed because of the large amount of current being sent into the primary coil and also the magnetic field coupling onto the circuitry. However, the copper cladding is not the best option for circuit layout because many of the circuit components protrude and act as antennas for the magnetic fields. After the initial prototype was finalized, a printed circuit board was designed, that reduces magnetic field coupling onto the circuit with the use of surface mount components, and creates a more controlled environment with parasitic capacitance reduction and mechanical stability.

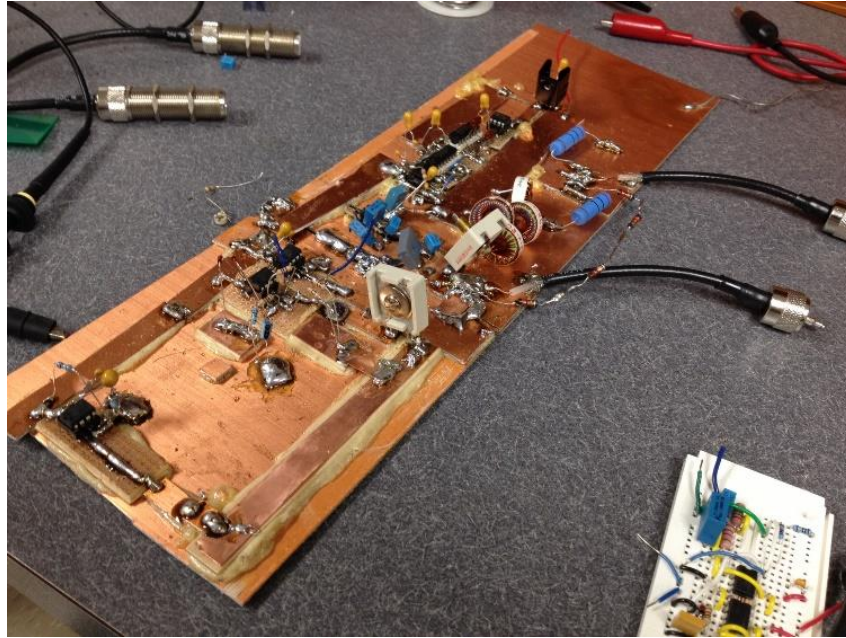


Figure 23: Copper Clad Prototyping

The primary coil was designed so that the magnetic field would uniformly occupy the cage of the rodent. Instead of using just one coil, where the magnetic field is concentrated at the center, a Helmholtz coil was used where the magnetic field is uniform and concentrated in a region between the two coils, separated as shown in Figure 24. Creating a region where there is a uniform magnetic field allows the implant to be successfully powered while the rodent is moving throughout the area of the cage, assuming the implant coils are parallel to the primary coil. In this prototype, only one set of coils was used, but it would be a simple matter to add additional coils at orthogonal orientations so the implant would be operational regardless of the position of the rodent. The implementation of the Helmholtz primary coil and the cage structure is shown in Figure 25. The magnetic field strength at the center point between the Helmholtz primary coil

can be derived using the Biot-Savart Law for a single wire loop along the z-axis, as in equation 2.3.

$$B(x) = \frac{\mu_0 n I R^2}{2(R^2 + x^2)^{\frac{3}{2}}} \quad (2.3)$$

- $R$  = Coil radius in meters
- $x$  = Coil distance to point in meters
- $I$  = Coil current in amperes
- $\mu_0$  = Permeability of freespace ( $8.85 \times 10^{-12} \text{ m}^{-3} \text{ kg}^{-1} \text{ s}^4 \text{ A}^2$ )

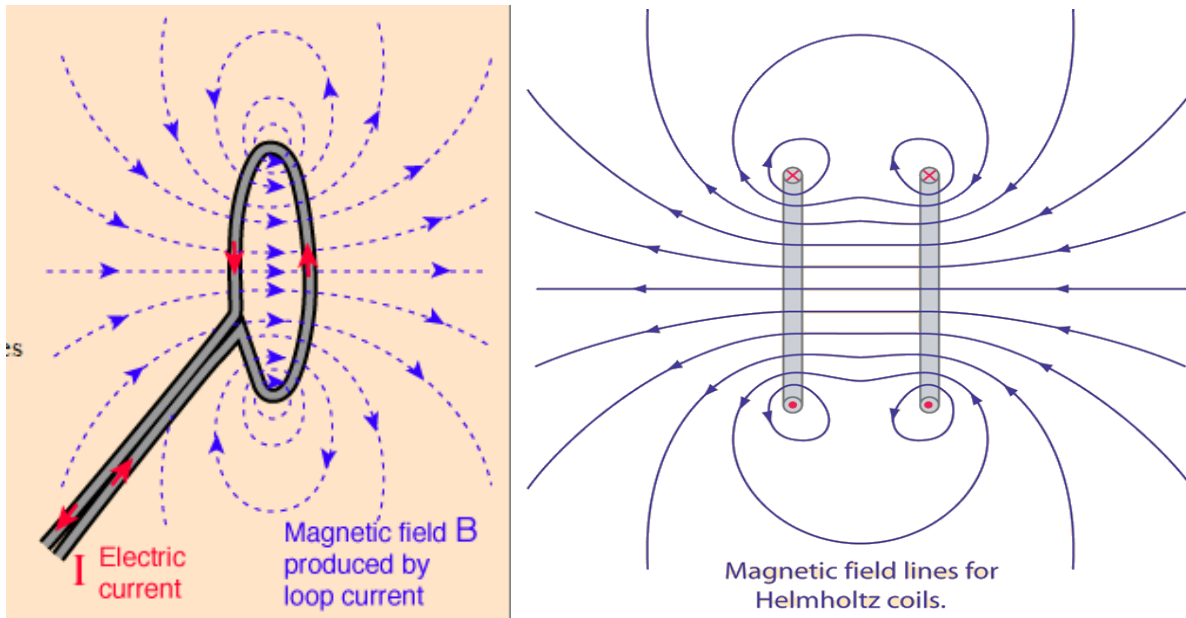


Figure 24: Magnetic Field of Single Loop and Helmholtz Coil [9][10]

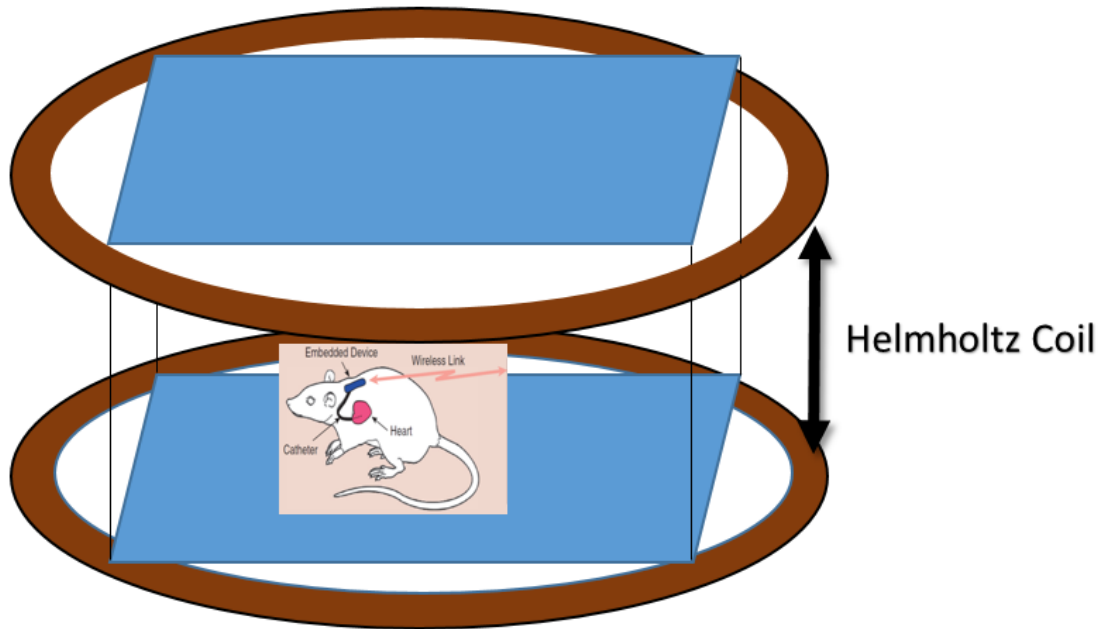


Figure 25: Cage Structure

If the distance between the two coils in the primary coil is the same as the radius of each coil, then the magnetic field in the region between is relatively homogenous. The homogenous magnetic field strength at the midpoint between the two coils of the primary coil can then be derived from equation 2.4 where  $x$  is now equivalent to the coil radius as shown below.

$$\left(\frac{8}{5\sqrt{5}}\right) \frac{\mu_0 n I}{R} \quad (2.4)$$

- $n$  = The number of turns of each coil



In the implemented design, a coil radius and equivalent distance of separation between the coils of 17.49cm was chosen due to the similarity in size of a small mouse cage as shown below in Figures 26 and 27. The primary coil is shielded in a copper covered enclosure to prevent magnetic field noise interference on the receiver circuitry, as shown in Figure 28. The penetration depth,  $\delta_p$ , of the magnetic fields can be calculated from equation 2.5.

$$\delta_p = \frac{1}{\sqrt{\pi f \mu_0 \sigma}} \quad (2.5)$$

- $\sigma$  = conductivity of copper
- $f$  = frequency of the fields

The penetration depth of the fields in copper was calculated to be 24.95um at the operational frequency of 6.78MHz.

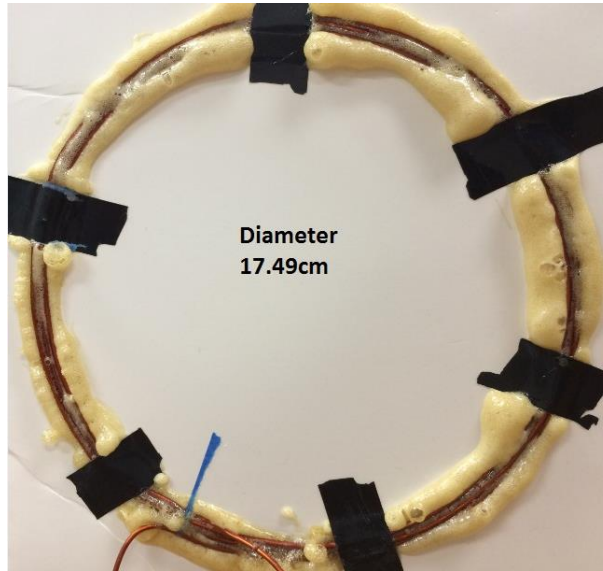


Figure 26: Helmholtz Coil Diameter

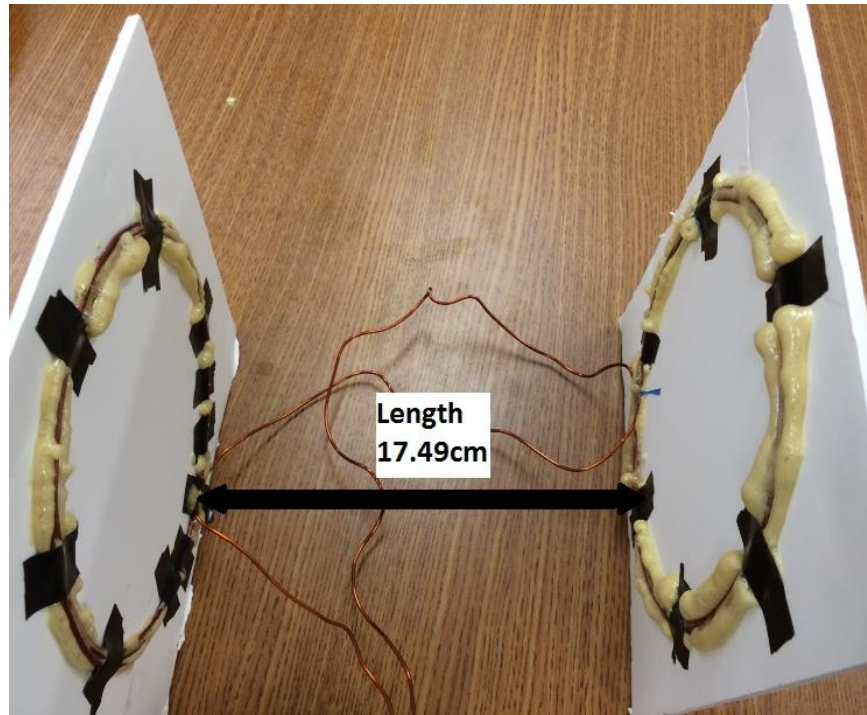


Figure 27: Helmholtz Coil Separation Distance



Figure 28: Copper Shielded Enclosure

### 2.4.2 Implant Design

The implant was designed on a printed circuit board with dimensions shown in Figure 29. The secondary power coil and transmitter coil are circular planar coils with turns distributed all the way to the center as shown in Figure 30. This coil structure was chosen because of the increased volumetric efficiency versus circular coils with turns concentrated on the circumference. The ratio of power delivered to the secondary coil and overall power consumption is given in equation 2.6 where  $Q_1$  and  $Q_2$  are the quality factors of the primary and secondary coils respectively. The  $k$  value is the coupling coefficient between the two coils and is given in equation 2.7 where  $L_a$  and  $L_b$  are the inductances of the primary and secondary coils and  $M_{ab}$  is the mutual inductance between them [11].

$$\eta_{12} = \frac{1}{1 + \frac{1}{k^2 Q_1 Q_2}} \quad (2.6)$$

$$k = \frac{M_{ab}}{\sqrt{L_a L_b}} \quad (2.7)$$

For circular planar coils with turns distributed all the way to the center, the coupling coefficient  $k$  is higher than for coils with turns distributed at the circumference, according to the derivation in reference [11]. An increase in  $k$  leads to an increase in  $\eta_{12}$  and the overall power efficiency, as shown in Figure 31, where tests have been done between primary coil and secondary coil of equivalent radius and inductance. In case (1), the coils have 4 turns distributed to the center whereas case (2) has 6 turns distributed to the center and has the highest power efficiency. In case (3), there are 3.55 turns distributed only along the circumference of the coil and has the lowest power efficiency. In reference [11], it was shown that the  $Q$  factors decrease when the coil

turns are distributed to the center, but the overall power efficiency increases because of the increase in the coupling coefficient  $k$ .

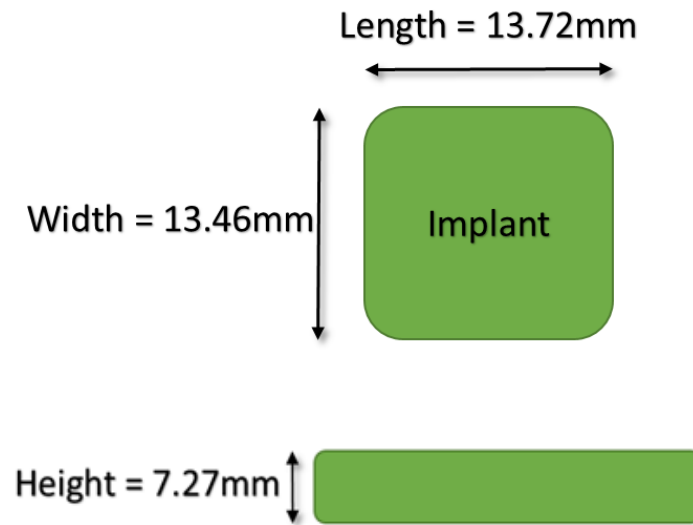


Figure 29: Implant Dimensions

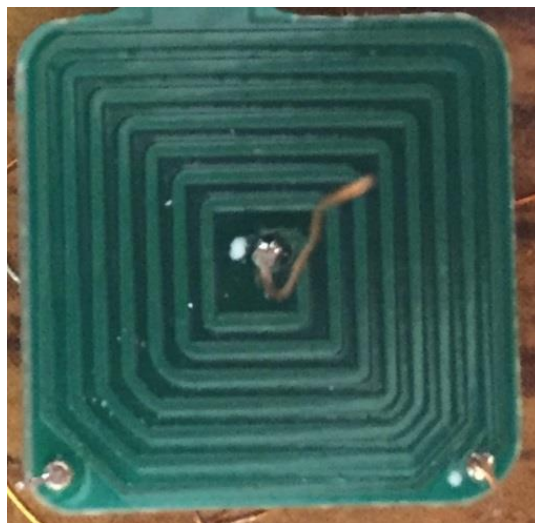


Figure 30: Implant Coil Structure

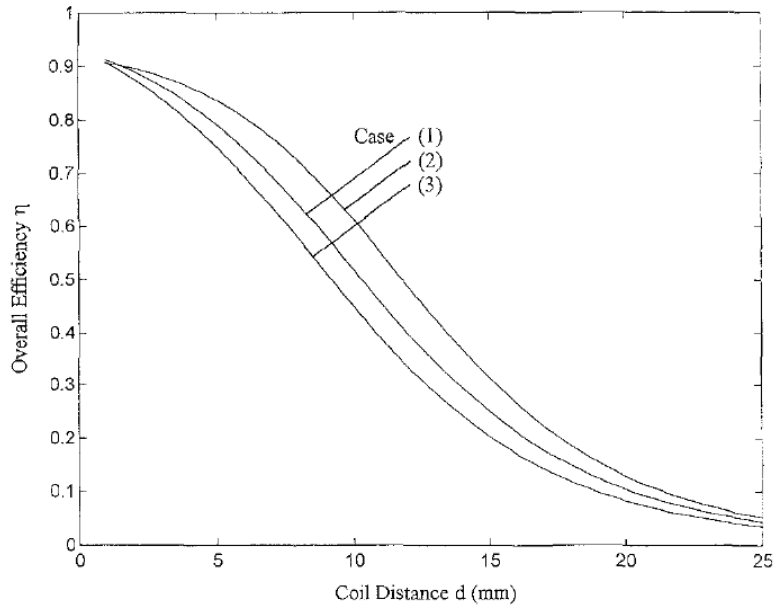


Figure 31: Overall Coil Efficiency with respect to Coil Distance

## 2.5 Temperature Data

Temperature data was taken from the internal temperature sensor that is located in the MCU. The temperature data is calibrated into Fahrenheit using equations suggested by the manufacturer and sent to the base station as an integer.

## Chapter 3: Verification and Results

### 3.1 Measurement Analysis

Figures 32 and 33 show the outputs of the oscillator circuit, where the 13.56MHz signal from the crystal oscillator output is divided to 6.78MHz after the D-Flip Flop stage. The output of the gate driver shows a 6.78MHz square wave with a slew rate of 160V/us. The ringing is probably due to unwanted parasitics and is not a major issue because the class E power amplifier efficiency is determined by transistor on and off state switching time. Adding a low pass filter to smooth out the ringing could potentially degrade power amplifier efficiency because the square wave slew rate may decrease.

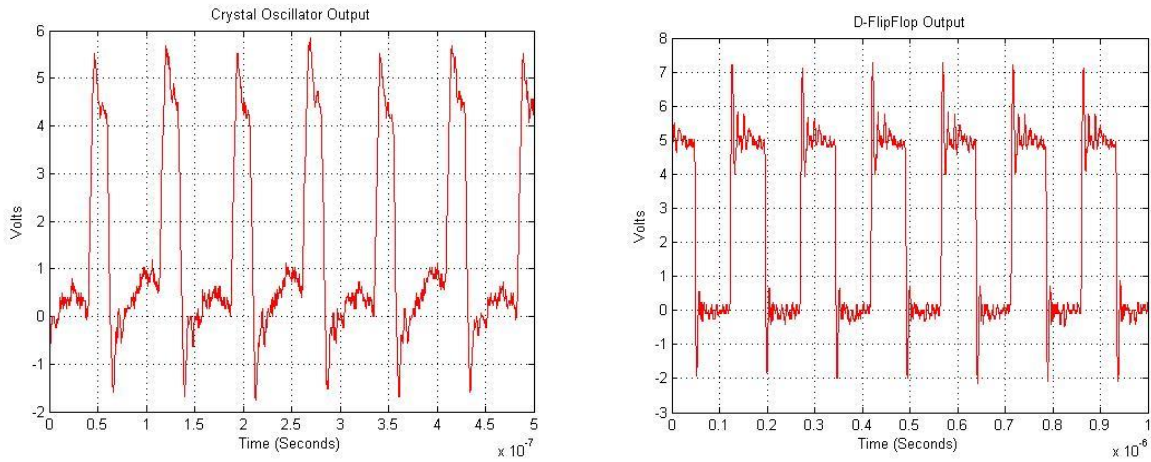


Figure 32: Crystal Oscillator and D-FlipFlop Output

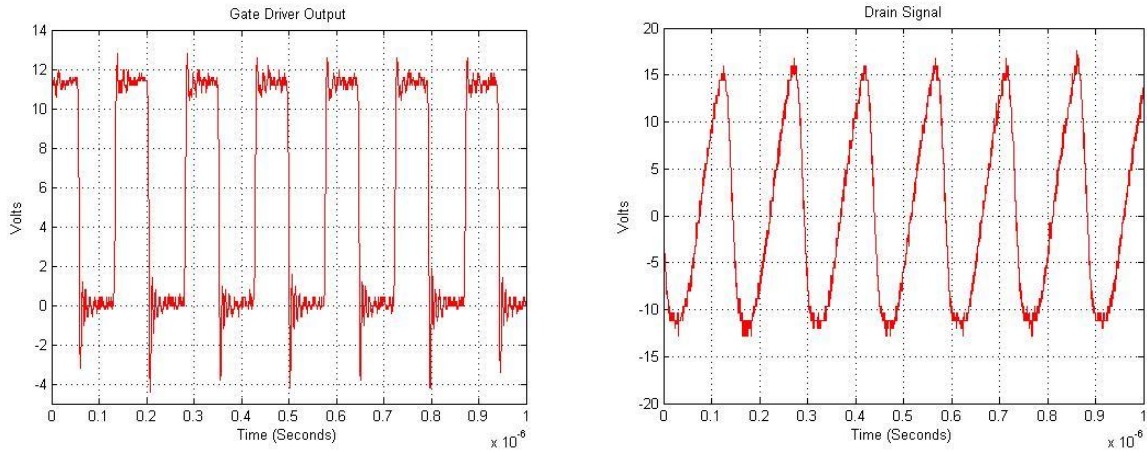


Figure 33: Gate Driver and Drain Signal Output

The drain signal output, shown in Figure 33, drops below 0 volts, which decreases the efficiency of the power amplifier because power is being dissipated in the transistor. A possible solution could be to add a diode from the drain (cathode) to ground (anode) in order to prevent this negative voltage at the drain.

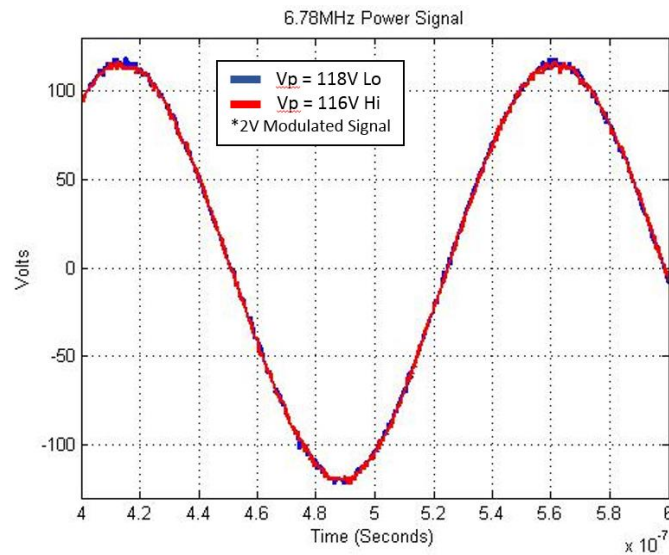


Figure 34: 6.78MHz Amplitude Modulated Power Signal



The power signal from the primary coil has a maximum amplitude of 120V when 6W of power is consumed by the power amplifier. The modulated power signal taken from the primary coil shows a 2V amplitude difference when the data signal is high (red), which drops the amplitude and when the data signal is low (blue) shown in Figure 34. This measurement was taken when the implant was 1cm away from the Helmholtz coils. The power signal is reduced by 96.6% in order to satisfy the linear input range of the operation amplifiers and half-wave rectified as shown in Figure 35.

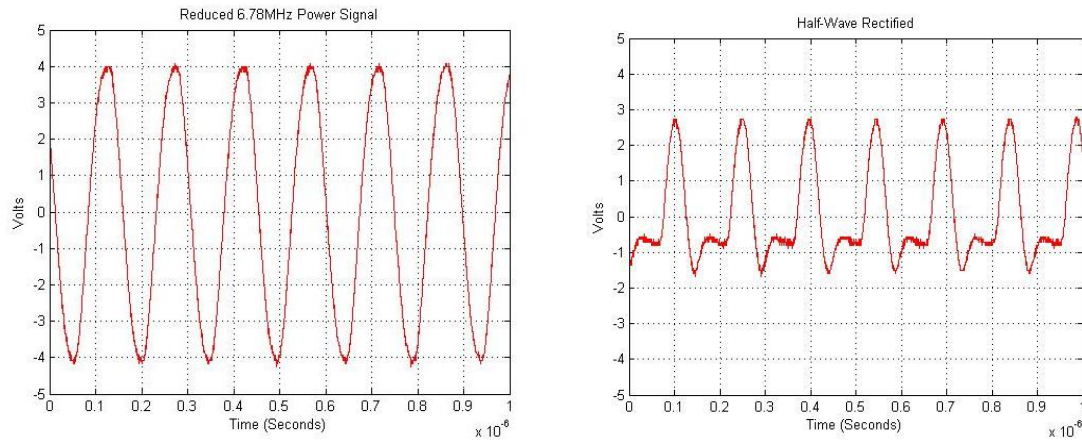


Figure 35: Reduced 6.78MHz Power Signal and Half-Wave Rectified Output

After rectification, the 10Hz data signal is demodulated as shown in Figure 36. The data signal can barely be seen as it is still smaller in amplitude versus the 6.78MHz carrier signal.



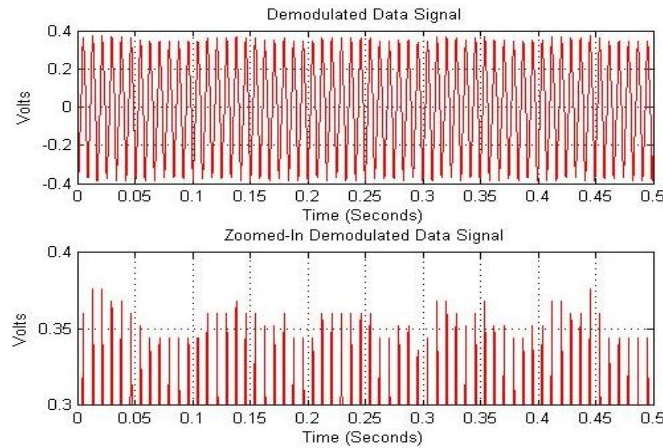


Figure 36: Demodulated Data Signal

After signal conditioning, the 10Hz square wave data signal can be seen clearly in Figure 37. There is noise riding on the peaks of the square wave, which was determined to be 60Hz and 120Hz mains power-line noise and the 6.78MHz carrier frequency that is coupled to the ground plane as shown in the FFT of the output data signal in Figure 38. The mains line noise can be high pass filtered in the analog domain once the data transmission rate is increased or digitally filtered. The 6.78MHz signal can also be filtered out in the digital domain.

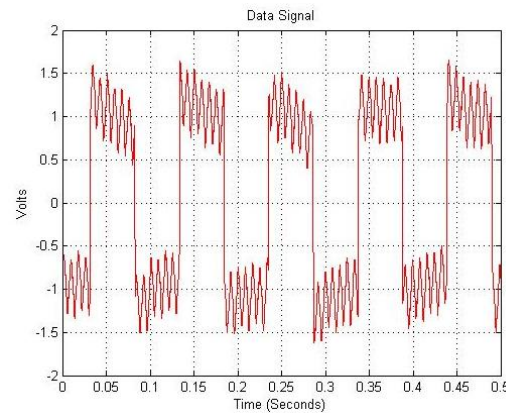


Figure 37: Data Signal

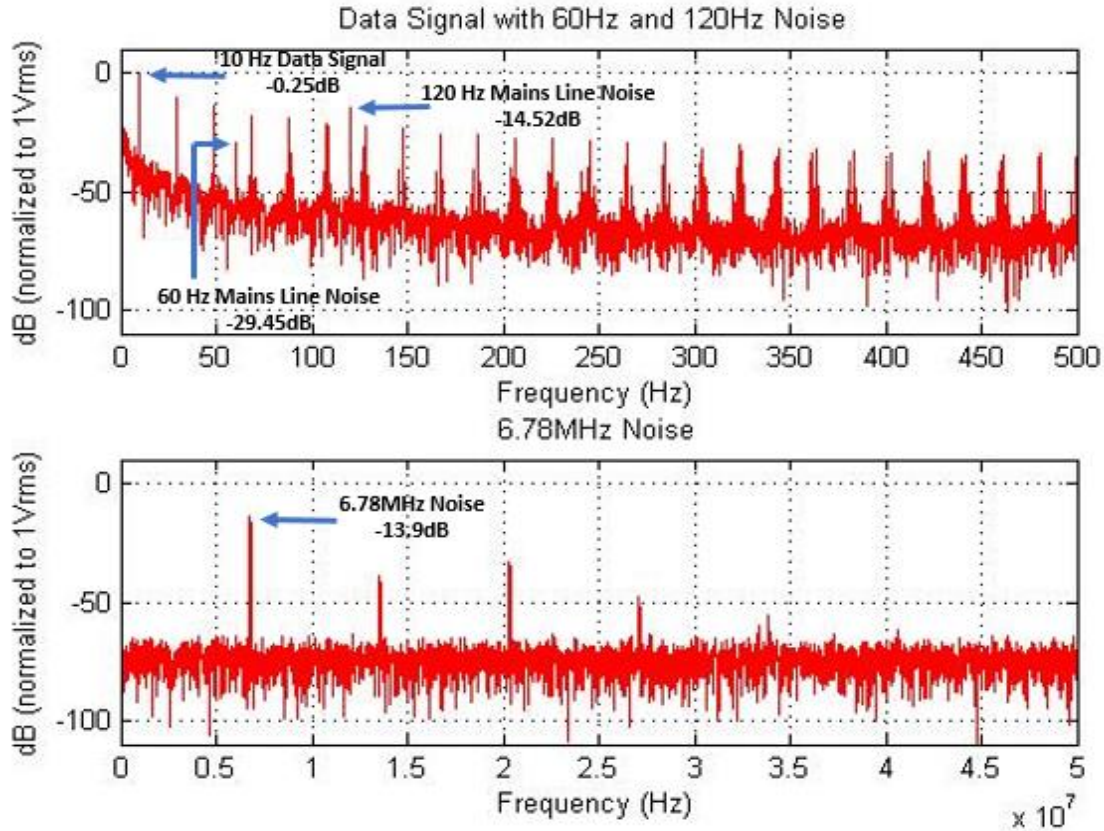


Figure 38: FFT of Data Signal with 60Hz, 120Hz, and 6.78MHz Noise

Tuning of the primary coil was done by adjusting the series LC tank capacitance until the power signal seen on the primary coil was maximum in amplitude. The implant secondary coil and transmitter coil were tuned by adjusting the parallel LC tank capacitance until the maximum impedance was reached at the resonant frequency of 6.78MHz. This proved to be more difficult as the coils actually proved to be tuned to 7.12MHz which leaves room for optimization in this area as shown in Figure 39. The series and parallel LC tank capacitances are adjusted with the use of variable capacitors.

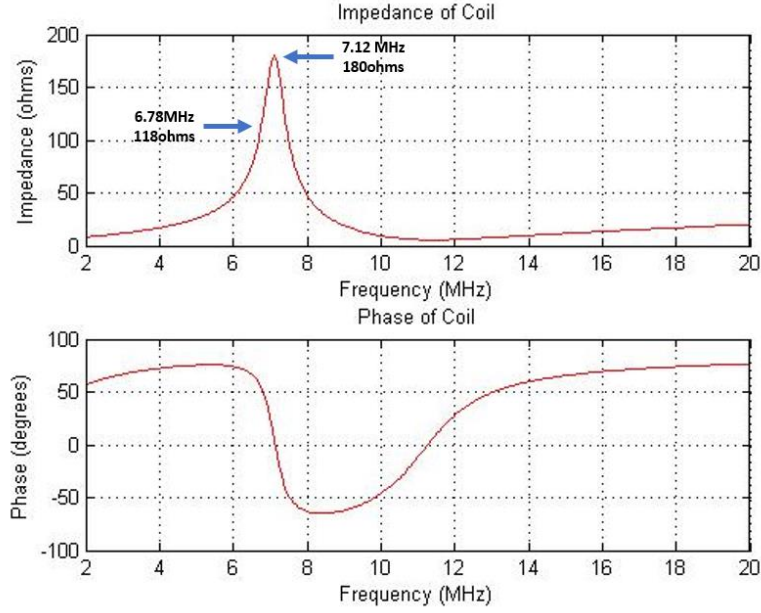


Figure 39: Implant Coil Magnitude and Phase Plot

### 3.2 Range and Power Consumption

The implant was successfully powered and run throughout the 5350cc space allotment of the Helmholtz coils. Total power consumption is calculated using equation 3.1 where  $I$  is the current drawn by the circuit and  $V$  is the supply voltage.

$$P = VI \quad (3.1)$$

The base station circuit draws 500mA of current during operation and consumes a total power of 6W with the use of a 12V supply. The communication from the implant to the base station was also successful throughout the space allotment. However, the gain of the receiver circuit needs to be increased as the implant comes closer to the middle of the Helmholtz coils (6cm away) where the magnetic field strength is weakest. The gain can be adjusted depending on the maximum

distance the implant will be from the Helmholtz coil, which depends on the height of the rodent, structure of the cage, and the positioning of the coils in the cage. The implant draws 4.1mA while it is processing and transmitting temperature data and consumes a total power of 10.25W with the use of a 2.5V supply.

### 3.3 Noise Analysis

The Shannon-Hartley Theorem in equation 2.6, calculates the theoretical limits on the information rate that can be sent through our channel that will provide accurate data.

$$C = B \log_2(1 + \frac{S}{N}) \quad (2.6)$$

- C = Channel capacity in bits/second
- B = Bandwidth
- S = Signal Power
- N = Noise Power

The current design allows for a channel capacity of 5.835 kbits/second with bandwidth of 1560Hz before digital filtering. Notice that the data signal is a rectangular-shaped, pulse which is composed of not just one tone, but many sine wave tones as shown in the FFT in Figure 38. Due to multiple signal frequencies contributing to the data signal, equation 2.7 is more commonly used to calculate the signal to noise ratio,  $S_n$ .

$$S_n = \frac{E_b R}{N_o B} \quad (2.7)$$

- $E_b$  = Energy per bit
- $N_0$  = Power spectral density
- $R$  = Clock frequency

$(E_b R)$  the energy per bit multiplied by the number of bits per second yields the signal power.

Whereas,  $N_0 B$  is the noise power spectral density ( $V_{\text{rms}}^2/\text{Hz}$ ) multiplied by the bandwidth, which gives the noise power. Notice that the bits per second,  $R$ , must be much less than the bandwidth or else there will be attenuation of the sinusoidal waveforms that make up the rectangular shaped data signal [4]. With this noise level, we could potentially achieve a data rate of 5835 bits/sec.

The data rate of 10 bits/sec is far below our bandwidth limit of 1560Hz, but must be considered for future designs with increased data rate. When the data rate is increased, the bandwidth must also be increased to prevent attenuation of the signal as stated above. However, as the bandwidth increases the signal to noise ratio decreases creating a tradeoff between bandwidth and signal to noise ratio when optimizing for the highest theoretical channel capacity. The maximum theoretical channel capacity can be further optimized with digital filters and other digital signal processing techniques.

## Chapter 4: Conclusion

### 4.1 System Performance

The wireless power transmission and communication system for rodents was designed to miniaturize implantable devices for rodents by using an inductive power link as an alternative to battery power. The impedance modulation method of communication reduces power and size of the implant eliminating the need for a bulky antenna. Another benefit is that without the battery and antenna, the weight of the implant is significantly reduced. The miniaturized implant will not impede the movement and lifestyle of the rodents as much, providing a more normal environment for physiological measurements. The previously stated design objectives were achieved in the system, as shown in Table 3.

Table 3: Achieved Design Objectives

	Target	Achieved
Size	<1.4cc	1.34cc
Operational Frequency	6.78MHz	6.78MHz
Data Frequency	10Hz	10Hz
Power Consumption (while transmitting)	<20mA	4.1mA (10.25mW)
Cage Volume	5350cc	5350cc
Communication Channel	Simplex	Simplex

Most notable of the design objectives is that the small size of the implant and the amount of power consumed compared to other devices on the market. However, the measurements from the system revealed that many design areas can be optimized. The 6W of power consumed by the

base station can be reduced with more efficient design of the power amplifier and potential coil structure changes to improve the coupling coefficient. Also, the implant secondary and transmitter coil are not tuned exactly to the operational frequency of 6.78MHz. The noise on the output signal from mains line noise and the 6.78MHz carrier frequency can be filtered out for better signal to noise ratio.

## **4.2 Future Directions**

### **4.2.1 Data Frequency**

In order to maximize the data transmission rate, the filter cutoffs in the signal conditioning block will need to be increased so that there will be no attenuation of the data signal, as described previously in the noise analysis section of chapter 3. This will allow the mains power-line noise to be more easily filtered out in the analog domain as well.

### **4.2.2 Communication Protocol**

After the data frequency is optimized, a communication protocol needs to be developed in order for the base station MCU to accurately decode the data. A possible solution would be to use an asynchronous serial interface, where the clocks on the base station MCU and implant MCU are running at the same frequency but can be out of phase. The base station will sample on each rising edge of the clock cycle. The temperature range is -256 to 255 degrees Fahrenheit, and the measurement resolution is 1 degree. Therefore, the communication channel needs to transmit 9 bits for each sample. If the implant sends 9-bits of data to represent a temperature value in Fahrenheit, the base station needs to know the beginning and end of the data bits. This can be

done by providing a start bit ST and a string of nine data bits, parity and a stop code SP as shown in Figure 40. The parity bit PAR is used for error detection. When the stop code is seen by the base station and the start bit goes low, the beginning of the 9-bits of data can be read. The data rate for this communication protocol is sufficient for temperature measurements.

ST	b0	b1	b2	b3	b4	b5	b6	b7	b8	PAR	SP
----	----	----	----	----	----	----	----	----	----	-----	----

Figure 40: Communication Protocol

#### 4.2.3 Half-Duplex Communication

Communication from the base station to the implant will be important for developing a more efficient communication protocol, and for reprogramming of the implant MCU. A proposed method of communication is to tune and detune the series LC tank capacitor on the primary coil corresponding to the data that needs to be sent to the implant. The primary coil must not be detuned to the point where the implant is no longer powered. The tuning and detuning will amplitude modulate the power signal and will be received by the transmitter coil on the implant. Similar to the receiver on the base station, circuitry can be designed on the implant board in order to demodulate and condition the data signal.

#### 4.2.4 Automatic Gain Control

When the rodent is moving, the implant distance from the Helmholtz coil will change. Automatic gain control will allow the gain in the receiver to be adjusted in order to maintain a constant



amplitude for the data signal. The communication link will never be lost and the data signal will never exceed the input range of any of the circuit components.

#### **4.2.5 Alternative Coil and Cage Structure**

The Helmholtz coil is currently aligned vertically because the rodent will be on all four feet most of the time and the implant coil will be parallel with the Helmholtz coil. However, if the rodent stands on two feet or lays on its side then the implant will be inefficiently powered. It is possible to add one or more Helmholtz power coils to the cage in order to power the implant at all angles. Another possible option is to use a columnar dual-transmitter coil proposed in reference [12].

## References

- [1] Kochanek KD, Xu JQ, Murphy SL, Miniño AM, Kung HC, “Deaths: final data for 2009,” National vital statistics reports, 2011.
- [2] Loeffler K, Porterfield JE, Larson ER, Escobedo D, Escobar GP, Pearce JA, Feldman MD, and, Valvano JW, "Embedded Medical Devices: Pressure Volume Loops in Rodents," IEEE Potentials, November/December 2012.
- [3] Loeffler K, “Development of an Implantable System to Measure the Pressure-Volume Relationship in Ambulatory Rodent Hearts,” The University of Texas, Austin, December 2012.
- [4] Rahul Sarpeshkar *Ultra Low Power Bioelectronics* (Cambridge, UK: Cambridge University Press 2010).
- [5] *Crystal Oscillator Basics and Crystal Selection for rfPIC and PICmicro Devices*. (n.d.). Retrieved December 2, 2014, from <http://ww1.microchip.com/downloads/en/AppNotes/00826a.pdf>
- [6] Steve C. Cripps. *RF Power Amplifiers for Wireless Communications* (Norwood, MA: Artech House, 2006).
- [7] Behzad Razavi. *RF Microelectronics* (Upper Saddle River, NJ: Prentice Hall, 1998).
- [8] *EEVblog #469-Cochrowft-Walton Multiplier*. (n.d.). Retrieved December 2, 2014, from [http://youtu.be/ep3D\\_LC2UzU](http://youtu.be/ep3D_LC2UzU)
- [9] *Magnetic Field of Current Loop*. (n.d.). Retrieved December 2, 2014, from <http://hyperphysics.phy-astr.gsu.edu/hbase/magnetic/curloo.html>
- [10] *Helmholtz Coils*. (n.d.). Retrieved December 2, 2014, from <http://hyperphysics.phy-astr.gsu.edu/hbase/magnetic/helmholtz.html>
- [11] C. M. Zierhofer, E. S. Hochmair, “Geometric Approach for Coupling Enhancement of Magnetically Coupled Coils” *IEEE Transactions on Biomedical Engineering*, **43**, 708-714, 1996.
- [12] K. Eom, J. Jeong, T. Lee, J. Kim, Ju. Kim, S. Lee, S. Kim, “a wireless power transmission system for implantable devices in freely moving rodents,” *Med Biol Eng Comput*, **52**, 639-651, 2014.